Inorganic Chemistry

ARTICLE

pubs.acs.org/IC

Flexible and Hydrophobic Zn-Based Metal−Organic Framework

Ines Maria Hauptvogel,[†] Ralf Biedermann,[†] Nicole Klein,[†] Irena Senkovska,[†] Amandine Cadiau,[†] Dirk Wallacher,[‡] Ralf Feyerherm,[§] and Stefan Kaskel*[,†]

[†]Department of Inorganic Chemistry, Dresden University of Technology, Bergstrasse 66, D-01069 Dresden, Germany

[‡]Department Sample Environments (NP-H12), Helmholtz Centre Berlin for Materials and Energy, Hahn-Meitner-Platz 1, D-14109 Berlin, Germany

[§]Institute Complex Magnetic Materials (M-I1), BESSY II, Helmholtz Centre Berlin for Materials and Energy, Albert-Einstein-Strasse 15, D-12489 Berlin, Germany

Supporting Information

ABSTRACT: A zinc-based metal−organic framework $Zn_2(adb)_2(dabco)\cdot 4.5$ DMF (***K***) (DUT-30(Zn), DUT = Dresden University of Technology, adb = 9,10-anthracene dibenzoate, dabco =1,4-diazabicyclo[2.2.2]octane, DMF = *N*,*N*-dimethylformamide) was synthesized using a solvothermal route. This MOF exhibits six crystallographic guest dependent phases. Two of them were characterized via single crystal X-ray analysis. The as-synthesized phase ***K*** crystallizes in the orthorhombic space group *Fmmm*, with $a = 9.6349(9)$, $b = 26.235(3)$, and $c = 28.821(4)$ Å and consists of two interpenetrated pillar-layer networks with **pcu** topology. When the substance loses 0.5 DMF molecules per formula unit, a phase transition from the kinetic phase ***K*** to a thermodynamic phase ***T*** occurs. $Zn_2(adb)_2(dabco)\cdot 4$ DMF (***T***) crystallizes in the tetragonal space group *I4/mmm*, with $a = 19.5316(8)$ and $c = 9.6779(3)$ Å. During the evacuation the DUT-30(Zn) undergoes again the structural transformation to ***A***. The activated compound ***A*** shows the gate pressure effect in the low pressure region of nitrogen physisorption isotherm and has a BET surface area of 960 $m^2\ g^{-1}$ and a specific pore volume of 0.43 $cm^3\ g^{-1}$. Furthermore, DUT-30(Zn) exhibits a hydrogen storage capacity of 1.12 wt % at 1 bar, a CO_2 uptake of 200 $cm^3\ g^{-1}$ at −78 °C and 0.9 bar, and a *n*-butane uptake of 3.0 $mmol\cdot g^{-1}$ at 20 °C. The N_2 adsorption process was monitored in situ via X-ray powder diffraction using synchrotron radiation. A low temperature induced transformation of phase ***A*** to phase ***V*** could be observed if the compound was cooled under vacuum to −196 °C. A further crystalline phase ***N*** could be identified if the framework was filled with nitrogen at −196 °C. Additionally, the treatment of activated phase ***A*** with water leads to the new phase ***W***.

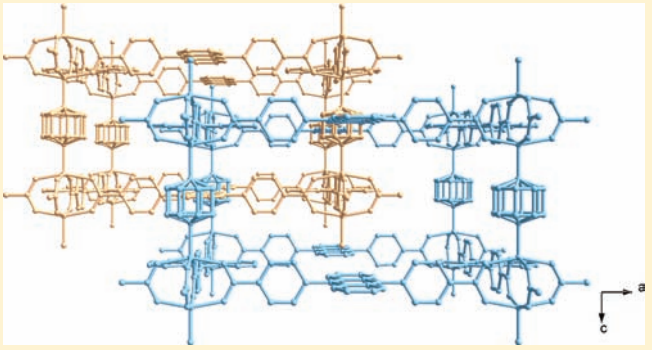

INTRODUCTION

In recent years a new class of microporous materials known as metal−organic frameworks (MOFs) or porous coordination polymers (PCPs) has attracted more and more not only fundamental, but also industrial, attention.[1−4] These compounds consist of rigid multidentate organic ligands (linker) and metal atoms or metal(-oxide) clusters (secondary building units (SBUs)).[1] The networks can reach high surface areas and pore volumes.[5−8] Due to the high porosity, the tunable pore size, and functionality, MOFs are predestinated for applications such as gas storage,[9−13] separation,[14−16] catalysis,[17−19] and drug delivery.[20,21]

MOFs with a dynamic behavior that, for instance, exhibit a guest induced structural change of the host lattice achieved considerable interest in literature, too.[22] Some established compounds in this vein are, for example, $M_2(1,4\text{-bdc})_2(dabco)$ (M = Zn, Cu, Co),[23−25] Al(OH)(1,4-bdc) (MIL-53),[26] $Ni_2(2,6\text{-ndc})_2(dabco)$ (DUT-8(Ni)),[27] and $Cu(bpy)(BF_4)_2(H_2O)_2\cdot(bpy)$ (ELM-11).[28] Such flexible frameworks are fascinating as they exhibit capability for recognition of certain molecules and excellent selectivity for guest inclusion and release. The term "breathing" MOFs was established for this class of porous coordination polymers. Among other MOFs, the pillared layer structures, such as $Zn_2(1,4\text{-bdc})_2(dabco)$, often show the breathing phenomenon. Kim et al. have demonstrated that the 1,4-benzene dicarboxylate (1,4-bdc) linker in $Zn_2(1,4\text{-bdc})_2(dabco)$ can be replaced by other dicarboxylates yielding a series of isoreticular MOFs.[29] Therefore, a longer ligand would lead to a structure with the same topology and possibly a higher surface area, gas adsorption capacity, and different flexible behavior.[30]

Indeed, with the bifunctional 9,10-anthracene dibenzoate (adb) as linker, synthesized via Suzuki coupling (for more details of the linker synthesis see Supporting Information (SI)),[31] it is possible to retain a structure analogue to $Zn_2(1,4\text{-bdc})_2(dabco)$. In parallel to our studies Zhou et al. discovered a copper paddle-wheel based MOF containing only adb as linker, namely

Received: May 5, 2011
Published: August 08, 2011

$Cu_2(adb)_2$ (PCN-18). PCN-18 is interdigitated by two sets of parallel 2D grid sheets.[31]

Here we report the synthesis, physisorption properties, and dynamic structural behavior of a zinc-based flexible metal−organic framework $Zn_2(adb)_2(dabco)$ (DUT-30(Zn)). Six crystallographic phases of the compound and its guest-induced dynamical interconversions are described. Two phases could be structurally characterized by single crystal X-ray analysis. The residual phases and phase transformations were investigated by in situ synchrotron powder diffraction. Furthermore, physisorption measurements of N_2, H_2, CO_2, H_2O, and *n*-butane were used to probe the pore accessibility of the activated compound.

EXPERIMENTAL SECTION

General Remarks. Zinc nitrate tetrahydrate (≥98.5%, Merck), 1,4-diazabicyclo[2.2.2]octane (dabco) (98%, Aldrich), and *N,N*-dimethylformamide (DMF) (≥99.5%, AppliChem) were used as received.

Powder X-ray diffraction data were collected on a Stoe STADI P powder diffractometer in transmission mode. Heating experiments were made in an argon atmosphere on X'pert panalytical diffractometer in HTK12 oven from AntonParr in the Laboratory of Oxide and Fluoride, University of Maine, Le Mans, France. In situ adsorption studies via synchrotron powder diffraction were performed at the 7T-MPW-MagS beamline, BESSY II, Helmholtz Centre Berlin. A special sample environment has been developed for this issue which is described in the Supporting Information. All powders were measured at a wavelength of 1.54 Å (8 keV).

Nitrogen and hydrogen low pressure physisorption isotherms were measured at −196 °C using a volumetric method in the range of 0.01−1 bar. The carbon dioxide adsorption was carried out at 0 °C and −78 °C. These adsorption isotherms were measured with a Quantachrome Autosorb1C apparatus. To quantify the nitrogen adsorption capacity after resolvatization and stability experiments a Quantachrome Quadrasorb *SI* was used for N_2 adsorption measurements. Measurement of *n*-butane adsorption was recorded using a microbalance (B111, Setaram) and water adsorption isotherms were measured using a Quantachrome Hydrosorb 1000 apparatus at 25 °C. For all adsorption measurements 50−100 mg of sample were used. Prior to the sorption measurements, the samples were evacuated at 120 °C for 20 h. A complete activation is reached at 180 °C but the adsorption amount does not increase any more. Only the PXRD pattern changes slightly. Thermogravimetric analyses were carried out using a Netzsch STA 409 PC Luxx thermal analyzer. Infrared spectra (IR) were recorded in diffuse reflectance geometry using a Nicolet Magna 550 Series II (Thermo Fisher Scientific Inc., Waltham, MA, USA) between 650 and 4000 cm^{-1}. Elemental analyses were performed with CHNS 932 elemental analyzer (LECO).

Synthesis of $Zn_2(adb)_2(dabco)$ (DUT-30(Zn)). $Zn_2(adb)_2(dabco)\cdot 4.5$ DMF (***K***). A mixture of $Zn(NO_3)_2\cdot 4\ H_2O$ (0.137 g, 0.52 mmol), H_2adb (0.219 g, 0.52 mmol), and dabco (0.029 g, 0.26 mmol) was suspended in DMF (25 mL) and heated in a 50-mL Teflon-lined autoclave at 120 °C for 48 h. The white crystalline precipitate (Figure S3a) was collected, washed with DMF, and dried under reduced pressure at room temperature for 1 h (0.221 g, yield: 62%).

Elemental analysis for $[Zn_2(C_{28}H_{16}O_4)_2(C_6H_{12}N_2)]\cdot 4.5$ DMF: calcd. (%): C 64.55, H 5.42, N 6.48; found (%): C 64.1, H 5.4, N 6.1. IR: ν = 3047 (w), 2915 (m), 2844 (m), 1938 (w), 1816 (w), 1689 (vs), 1650 (m), 1610 (w), 1558 (m), 1511 (m), 1423 (s), 1400 (m), 1259 (m), 1176 (m), 1097 (m), 1060 (m), 1020 (m), 944 (m), 925 (m), 844 (m), 811 (m), 781 (m), 740 (m), 711 (m), 665 (m) cm^{-1}.

$Zn_2(adb)_2(dabco)\cdot 4.5$ DMF (***K***)—synthesis of crystals for single crystal structure analysis. A mixture of $Zn(NO_3)_2\cdot 4\ H_2O$ (6.5 mg, 0.025 mmol), H_2adb (10.3 mg, 0.025 mmol), and dabco (1.4 mg, 0.0125 mmol) was suspended in DMF (3.5 mL) and five drops of formic acid were added. The reaction mixture was heated in a Pyrex tube at 120 °C for 48 h to yield light yellow needles (Figure S3b).

$Zn_2(adb)_2(dabco)\cdot 4$ DMF (*T*). To obtain **T** $Zn_2(adb)_2(dabco)\cdot 4.5$ DMF (***K***) was evacuated at room temperature for 20 h.

Elemental analysis for $[Zn_2(C_{28}H_{16}O_4)_2(C_6H_{12}N_2)]\cdot 4$ DMF: calcd. (%): C 64.96, H 5.30, N 6.14; found (%): C 64.4, H 5.5, N 5.86. IR: ν = 3048 (w), 2919 (w), 2844 (m), 1936 (w), 1812 (w), 1681 (s), 1558 (m), 1513 (m), 1469 (m), 1423 (s), 1396 (m), 1251 (w), 1176 (m), 1091 (m), 1056 (m), 1018 (m), 943 (m), 921 (m), 844 (m), 809 (m), 771 (m), 738 (w), 709 (w), 673 (m) cm^{-1}.

$Zn_2(adb)_2(dabco)$ (*A*). The sample of ***K*** or ***T*** was evacuated at 180 °C for 24 h to give ***A***.

Elemental analysis for $[Zn_2(C_{28}H_{16}O_4)_2(C_6H_{12}N_2)]\cdot 1.5\ H_2O$: calcd. (%): C 67.52, H 4.30, N 2.54; found (%): C 67.6, H 4.4, N 2.62. IR: ν = 3060 (m), 2913 (m), 2890 (w), 1922 (w), 1801 (w), 1714 (m), 1635 (v), 1548 (m), 1510 (m), 1467 (m), 1423 (s), 1174 (m), 1095 (m), 1054 (m), 1018 (m), 943 (m), 914 (w), 842 (m), 806 (m), 777 (m), 759 (m), 711 (m), 665 (m) cm^{-1}.

Single Crystal Structure Determination. Crystals of ***T*** and ***K*** were chosen under polarized light and prepared in Paraton-N oil (Hampton Research) and transferred into glass capillaries with a diameter of 0.3 mm. The data were collected on a STOE IPDS (Me_2adb), IPDS II (***K***), or a Bruker APEX II (***T***) single crystal diffractometer. All devices are operated with Mo Kα radiation (λ = 0.71073 Å, fine-focus sealed tube, graphite monochromator). The diffraction experiments were carried out at room temperature. Initially, a few hundred incidental reflections were collected and the cell parameters were determined. Complete data collection was performed with an optimized instrumental setup. Collected raw data were integrated with Lorenz- and polarization correction. Finally the data set was examined for systematic absences and the space group was determined. The unit cell has been refined with the integrated data. An initial structural model was determined by the use of the charge flipping algorithm.[32] Missing atoms were located via difference Fourier map. The model was improved by full matrix least-squares refinement with ShelXL until convergence.[33] The hydrogen atoms were positioned geometrically and refined using a riding model. Non-hydrogen atoms of the networks were refined with anisotropic temperature parameters. Application of the SQEEZE[34] routine in the PLATON software package produced a new intensity data set excluding the intensity contribution from disordered solvent molecules.

CCDC-804770 (***K***), -804771 (***T***), and -804772 (Me_2adb) contains the supplementary crystallographic data for this paper. These data can be obtained free of charge from the Cambridge Crystallographic Data Centre via www.ccdc.cam.ac.uk/data_request/cif or from the Supporting Information.

RESULTS AND DISCUSSION

Crystal Structure of $Zn_2(adb)_2(dabco)$ and Dynamic Transformation. $Zn_2(adb)_2(dabco)$ (DUT-30(Zn)) was obtained as a microcrystalline material via solvothermal synthesis using zinc nitrate as metal source, H_2adb and dabco as ligands, and DMF as solvent (Figure S3). It turned out that the synthesized coordination polymer shows guest-dependent crystal-to-crystal transformation. Finally we were able to characterize six different crystallographic phases of this MOF.

$Zn_2(adb)_2(dabco)\cdot 4.5$ DMF could be obtained in the form of crystals suitable for single crystal X-ray analysis when formic acid was added to the reaction mixture (Figure S3b). We name this phase the kinetic phase (***K***).

K crystallizes in the space group *Fmmm*, with a = 9.6349(9), b = 26.235(3), and c = 28.821(4) Å (For more information, see

Table 1. Crystal Data and Structure Refinement Information for DUT-30(Zn) (*K*) and DUT-30(Zn) (*T*)

	DUT-30(Zn) (*K*)	DUT-30(Zn) (*T*)
empirical formula	$C_{62}H_{44}N_2O_8Zn_2$	$C_{62}H_{44}N_2O_8Zn_2$
formula weight	537.87	537.87
temperature	293(2) K	293(2) K
wavelength	0.71073 Å	0.71073 Å
crystal system	orthorhombic	tetragonal
space group	*Fmmm* (no. 69)	*I4/mmm* (no. 139)
unit cell dimensions	a = 9.6349(9) Å	a = 19.5316(8) Å
	b = 26.235(3) Å	c = 9.6779(3) Å
	c = 28.821(4) Å	
volume	7285.3(15) Å^3	3692.0(2) Å^3
Z	8	4
density (calcd)	0.981 g·cm^3	0.993 g·cm^{-3}
absorption coefficient	0.701 mm^{-1}	0.691 mm^{-1}
F(000)	2216	1108
crystal size	0.5 × 0.15 × 0.15 mm^3	0.22 × 0.16 × 0.06 mm^3
θ range for data collection	1.41 to 25.79°	2.09 to 25.99°
index ranges	$-8 \le h \le 11$	$-19 \le h \le 24$
	$-22 \le k \le 31$	$-23 \le k \le 24$
	$-31 \le l \le 34$	$-10 \le l \le 11$
reflections collected	4345	13141
independent reflections	1879 [R_{int} = 0.0579]	1063 [R_{int} = 0.0694]
completeness to θ	96.5%	99.8%
refinement method	full-matrix least-squares on F^2	full-matrix least-squares on F^2
data/restraints/parameters	1879/0/111	1063/9/72
goodness-of-fit on F^2	0.944	0.926
final R indices [$I > 2\sigma(I)$]	R_1 = 0.0600,	R_1 = 0.0396,
	wR_2 = 0.1365	wR_2 = 0.1142
R indices (all data)	R_1 = 0.0888,	R_1 = 0.0443,
	wR_2 = 0.1458	wR_2 = 0.1166
largest diff. peak and hole	0.909 and −0.632 e A^{-3}	0.317 and −0.375 e Å^{-3}

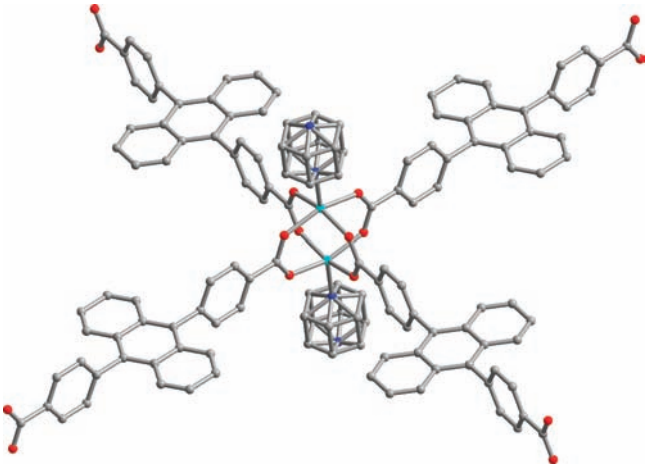

Figure 1. Paddle-wheel-unit of *K*.

Table 1) and is a typical layer-pillar-MOF. A square-planar 4,4-net is formed by Zn_2-paddle-wheel-SBUs whose equatorial coordination sites are occupied by the bidentate 9,10-anthracene dibenzoate anion (Figure 1). The phenylene rings of the adb linker in ***K*** are twisted exactly 90° to the anthracene unit. This is not the case in the crystal structure of Me_2adb. There the torsion angle between anthracene and phenylene amounts to 81.65° (for more details see SI). The axial coordination sites in ***K*** are ligated by dabco (1,4-diazabicyclo[2.2.2]octane), which acts as a pillar interconnecting the $Zn_2(adb)_2$-layers in [100] direction, and a net with **pcu** topology is formed. Due to the large size of the adb ligand, the pores are big enough for a second net which interpenetrates the first one. The individual nets in ***K*** are related by translations. The fractional centering vectors are 1/2 1/2 0 and 1/2 0 1/2.

When the substance is allowed to lose some of the solvent out of the pores (for more details see SI), an irreversible phase transition from ***K*** to a thermodynamic phase ***T*** ($Zn_2(adb)_2(dabco)\cdot 4$ DMF) takes place. The metastable ***K*** phase ($Zn_2(adb)_2(dabco)\cdot 4.5$ DMF) can be stabilized in a DMF atmosphere. ***T*** can be also synthesized directly, if a mixture of DMF and toluene is used as solvent during the solvothermal synthesis (Figure S4). The single networks of both phases are topologically equivalent to that of $Zn_2(1,4\text{-bdc})_2(dabco)$.[20]

The thermodynamic stable phase ***T*** crystallizes in the space group *I4/mmm*, a translation equivalent supergroup (index 2) of the kinetic phase ***K***. The diagram in Scheme 1 illustrates the relationship. The knot of the first net in ***T*** lies on the (0, 0, 0) position of the unit cell, the second net's knot lies in (1/2, 1/2, 1/2), as shown in Figure 2.

dx.doi.org/10.1021/ic200937u |*Inorg. Chem.* 2011, 50, 8367–8374

The dabco ligand in ***T*** lies on the 4-fold axis of the space group *I4/mmm* but has 3-fold point symmetry itself. Hence, it is disordered. The same is observed in ***K*** in *Fmmm*, where two mirror planes are orthogonally crossing through the 3-fold ligand.

In ***K*** there are two different pores. One has the dimension of 7.6 × 9.8 Å and the other is 6.3 × 11.3 Å. ***T*** shows just one kind of pore which is 7.0 × 10.5 Å big. Due to the bulkiness of the adb linker and the short pillar dabco ligand no third net can be embedded which leads to the relative large dimensions of the pores in comparison to other interpenetrated layer-pillar MOFs, like $Zn_2(adc)_2(bpe)$ (adc =4,4′-azobenzene dicarboxylate, bpe = *trans*-bis(4-pyridyl)ethylene) and $Zn_2(cnc)_2(dpt)$ (cnc = 4-carboxycinnamic acid, dpt = 3,6-di-4-pyridyl-1,2,4,5-tetrazine), which show 3-fold interpenetration due to the larger colinkers.[35] But not only the linker length is responsible for the degree of the interpenetration. Hupp and co-worker demonstrated that also the adjustment of linker bulkiness opens the possibility to control the degree of interpenetration in the pillar layered structures.[36]

Furthermore, the dynamic behavior increases if the interpenetrated networks have high mobility related to each other.

In Figure 3 structural superposition of both modifications (***K*** and ***T***) is shown. The additional solvent causes the change of network conformation, and symmetry lowering, resulting in distorted lattice of ***K***. Unfortunately, an exact localization of the solvent molecules in the pores by difference Fourier map could not be achieved because of strong disorder (see Experimental Section for details). The molecular formulas were determinate using elemental analyses.

The further removal of solvent from ***T*** or ***K*** induces again the structural transformation and another lattice is formed which we call the activated phase ***A***. The path from ***K*** to ***T***, further to ***A***, and finally to ZnO during the heat period is shown in Figure 4. Resolvatization of ***A*** using DMF resulted in recovery of ***T***. The phase ***K*** could not be obtained via resolvatization of ***A***.

The next phase transition could be observed when the DUT-30(Zn) was exposed to water. ***W*** was obtained after hydration of ***A*** or direct exchange of DMF in ***K*** or ***T*** with water. Surprisingly, the water molecules of ***W*** cannot be removed by heating (up to 150 °C) in vacuum. The sole possibility to achieve ***A*** from ***W*** is the competitive replacement of water with DMF to ***T*** and further evacuation. Though the ***K***−***T*** relation is monotropic, ***K*** is not accessible from ***W***.

A similar finding was made by Kitagawa et al.[37] The adsorption properties of topological equivalent of DUT-30, a **pcu** 2-fold interpenetrated layer-pillar network ($Zn_2(btdc)_2(bpy)$) (btdc = 2,2′-bithiophene-5,5′-dicarboxylic acid, bpy =4,4′-bipyridine)

Scheme 1. Lattice Constants and Group−Supergroup Relationship of the Monotropism of the DMF Solvate of $Zn_2(adb)_2(dabco)$

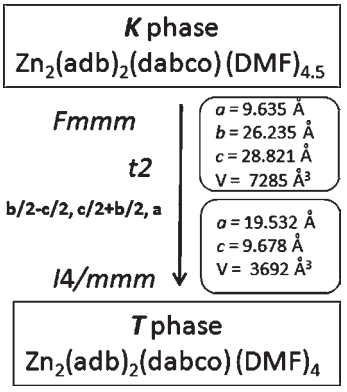

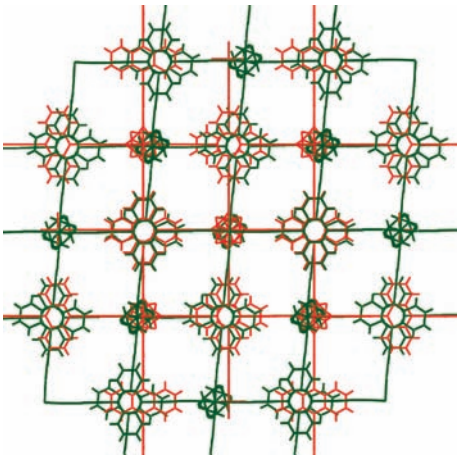

Figure 3. Structure overlay of ***K*** (green) and ***T*** (red). View perpendicular to the $Zn_2(adb)_2$-layers.

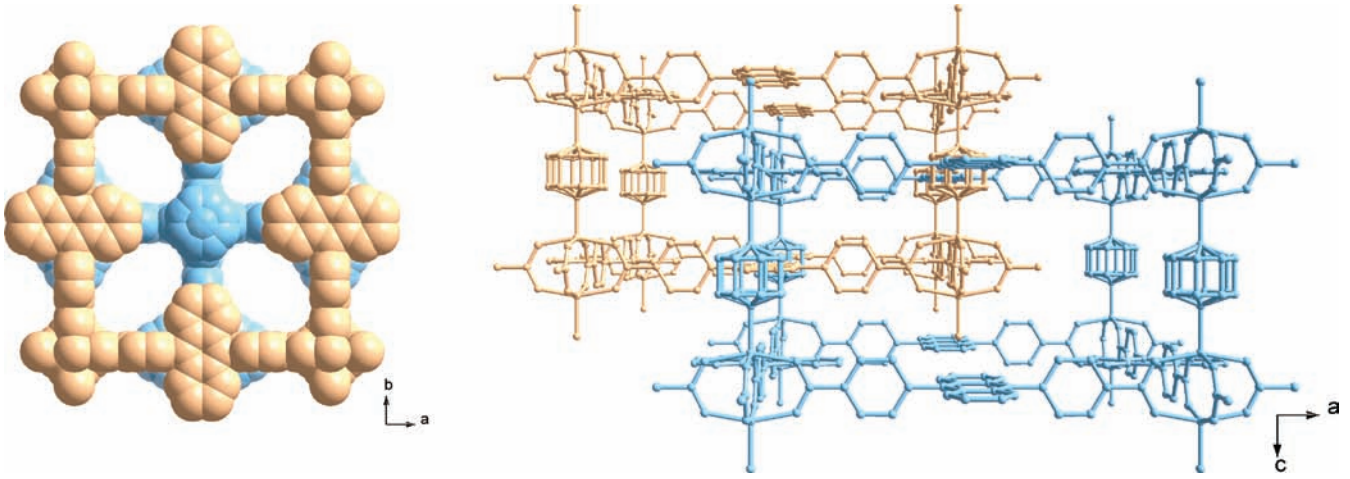

Figure 2. Left: Space filling packing diagram of the interpenetrated subnets; right: interpenetrated networks of ***T***.

dx.doi.org/10.1021/ic200937u |*Inorg. Chem.* 2011, 50, 8367–8374

were investigated via in situ synchrotron powder diffraction. This compound is built from MOF-building-blocks of lower point group symmetry and hence, the observed phases are not crystallizing in high symmetry space groups. Structurally, the authors came to the conclusion that the guest-stabilized squared pores in [001] direction are getting rhombohedrally distorted with changes in the guest load.

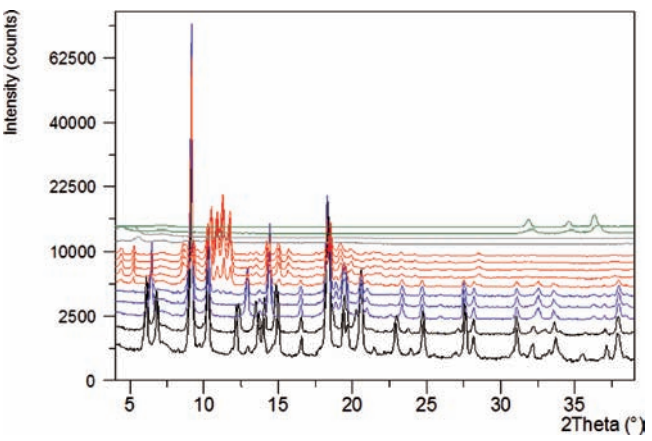

Figure 4. Powder XRD patterns of $Zn_2(adb)_2(dabco)$ during the heating process from ***K*** (black, 25−50 °C) to ***T*** (blue, 70−110 °C) and ***A*** (red, 130−270 °C), an amorphous phase (gray, 290−330 °C), and ZnO (green, 350−750 °C).

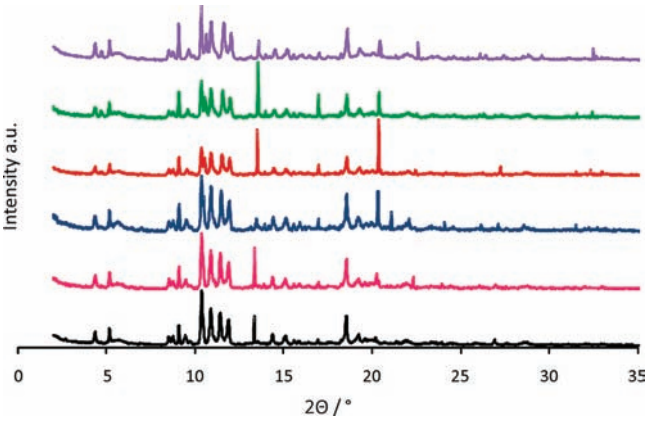

Figure 5. Powder XRD patterns of $Zn_2(adb)_2(dabco)$ during the cooling process from 27 °C (black) to −196 °C (violet).

To investigate the behavior of phase ***A*** during the gas adsorption, in situ synchrotron PXRD experiments were performed using synchrotron radiation on the 7T-MPW-MagS beamline at BESSY II (Berlin, Germany).

Interestingly, a further transformation takes place when ***A*** is annealed to −196 °C in vacuum—the phase ***V*** is formed. Figure 5 shows the transformation of ***A*** to ***V*** during the cooling procedure monitored via PXRD.

When nitrogen is dosed to the evacuated $Zn_2(adb)_2(dabco)$ sample at −196 °C, the ***V*** phase undergoes further transformation to the phase ***N*** (Figure 6). After desorption of gas and heating to room temperature the ***N*** phase transforms back to ***A***.

The attempts to solve the crystal structures of phases ***A***, ***V***, and ***N*** from the powder data were not successful because the symmetry of the compounds is too low and nearly all reflections overlap. Furthermore, a fundamental problem is the scattering part of the guest molecules.

Scheme 2 schematically illustrates all phases observed for DUT-30(Zn) and their transformation paths.

Adsorption Studies. To evaluate the porosity of DUT-30-(Zn), the physisorption measurements using N_2, H_2, CO_2, H_2O, and *n*-butane as adsorptive were carried out on the activated compound ***A***.

Due to the flexibility of the structure (3rd generation porous coordination compounds) a so-called gate-pressure effect is observed in the nitrogen adsorption isotherm of activated $Zn_2(adb)_2(dabco)$ (***A***) (Figure 7), thus in the range of $p/p_0 = 0-0.2$ the adsorption branch does not coincide with the desorption branch.[1] However, the BET surface area of the solvent-free framework of 960 m^2g^{-1}, calculated with multipoint BET method in the range of $p/p_0 = 0.03-0.1$, and the specific pore volume of 0.43 $cm^3\ g^{-1}$ (at 0.9 p/p_0) are lower as expected for elongated analogue of $Zn_2(1,4\text{-bdc})_2(dabco)$, due to the interpenetration.

The hydrogen adsorption isotherm of ***A*** measured at −196 °C is shown in Figure 8. The maximum hydrogen uptake is 1.12 wt %

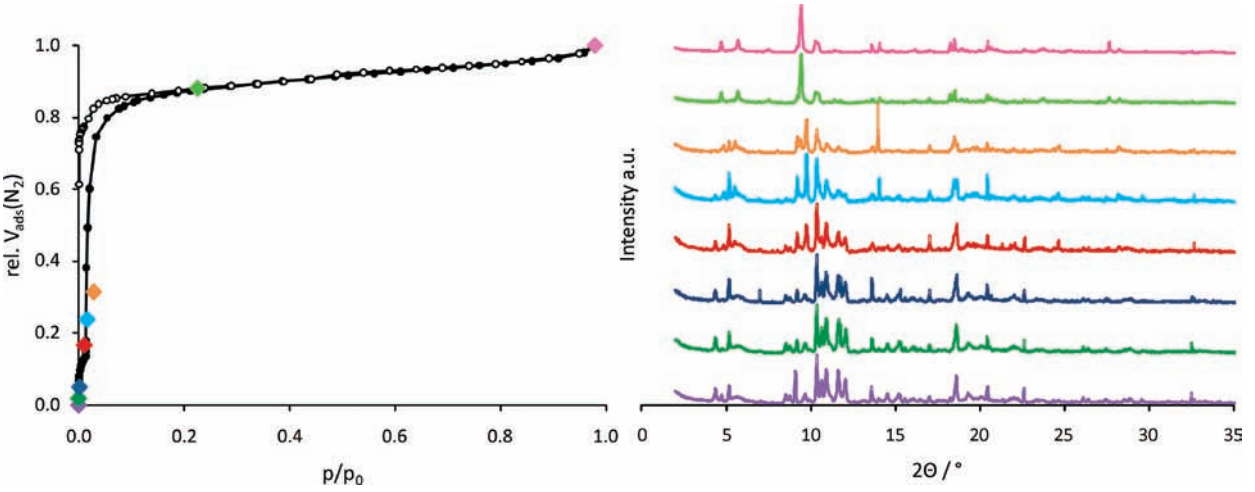

Figure 6. Left: Nitrogen adsorption isotherm of $Zn_2(adb)_2(dabco)$; right: powder XRD patterns of $Zn_2(adb)_2(dabco)$ while adsorbing nitrogen. The colored diamonds show which PXRD is measured at which point of the isotherm.

dx.doi.org/10.1021/ic200937u |*Inorg. Chem.* 2011, 50, 8367–8374

Scheme 2. Six Crystalline Phases of $Zn_2(adb)_2(dabco)$

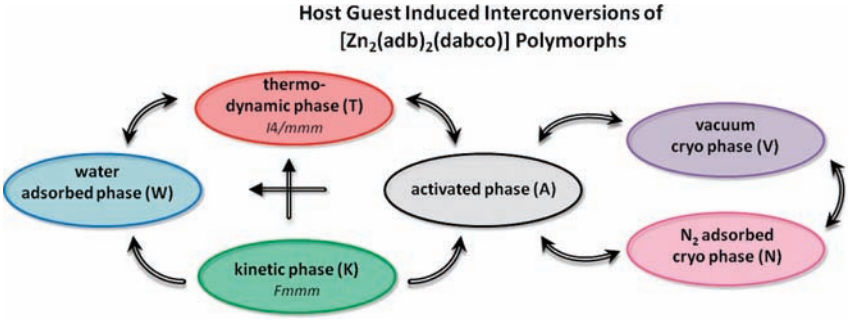

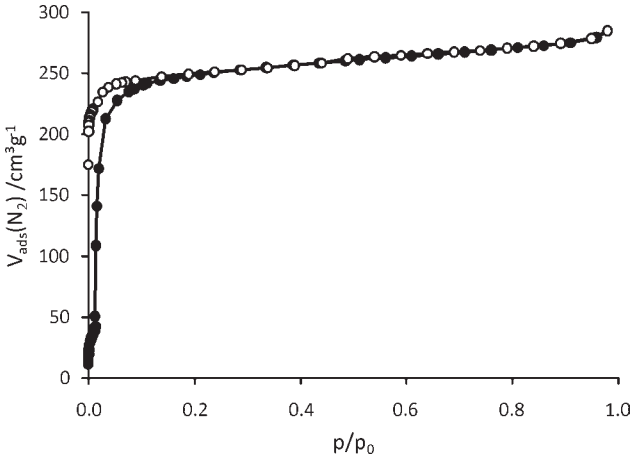

Figure 7. N_2 adsorption and desorption isotherms of $Zn_2(adb)_2$-(dabco) at −196 °C.

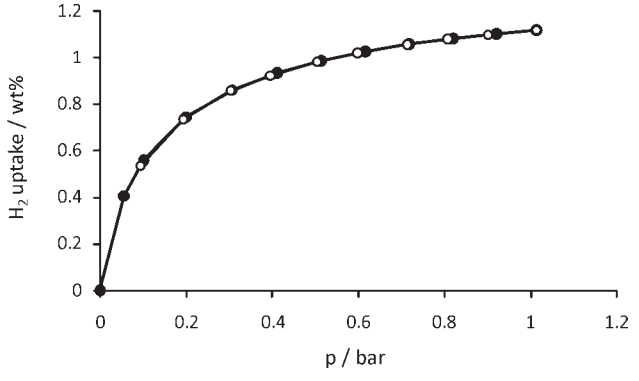

Figure 8. H_2 adsorption isotherm of $Zn_2(adb)_2(dabco)$ at −196 °C.

at 1 bar and is thus lower than for $Zn_2(1,4\text{-bdc})_2(dabco)$ (2.0 wt %)[20] due to the interpenetration of the networks.

The water adsorption properties of DUT-30(Zn) were studied and compared with other MOFs investigated earlier.[13] Due to the high polarity of the water molecule, information concerning hydrophobic or hydrophilic character of the substances (as well as concerning the stability against moisture) can be achieved. DUT-30(Zn) shows a water physisorption isotherm similar to ZIF-8, a highly hydrophobic and chemically stable zeolitic imidazolate framework[38] (Figure 9). The pore volume calculated at 0.95 p/p_0 amounts to 0.30 $cm^3\ g^{-1}$. Thus, DUT-30(Zn) is a

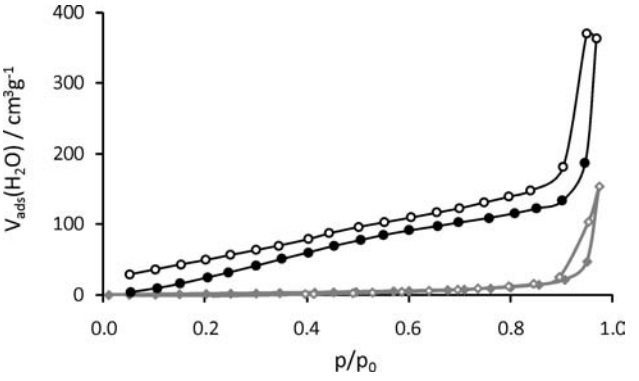

Figure 9. H_2O adsorption isotherms of DUT-30(Zn) (●) and ZIF-8 (♦) at 25 °C.

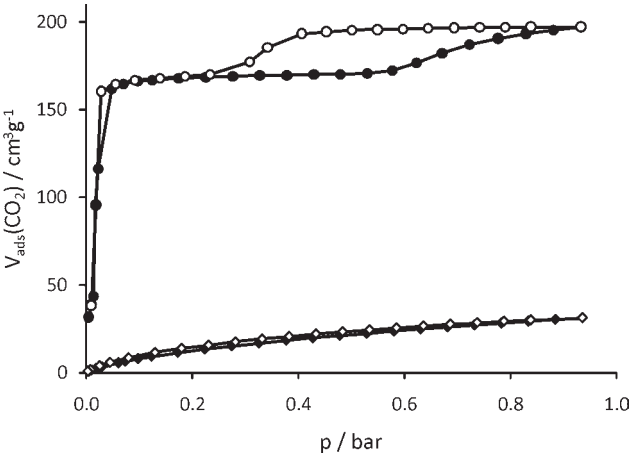

Figure 10. CO_2 adsorption isotherm of $Zn_2(adb)_2(dabco)$ at −78 °C (●) and 0 °C (♦).

promising hydrophobic MOF due to the larger pore size as compared to ZIF-8.

The CO_2 adsorption isotherms of ***A*** at 0 °C and −78 °C are represented in Figure 10. At −78 °C the CO_2 isotherm displays approximately the same progression as the N_2 isotherm; therefore, the gate-pressure effect can be observed and the BET surface area amounts to 970 $m^2\ g^{-1}$ (p/p_0 = 0.03−0.1) as well.

The CO_2 storage capacity of $Zn_2(adb)_2(dabco)$ is about 200 $cm^3\ g^{-1}$ at −78 °C and 0.9 bar and ca. 30 $cm^3\ g^{-1}$ at 0 °C and 0.9 bar which is comparable to other MOFs.

dx.doi.org/10.1021/ic200937u |*Inorg. Chem.* 2011, 50, 8367–8374

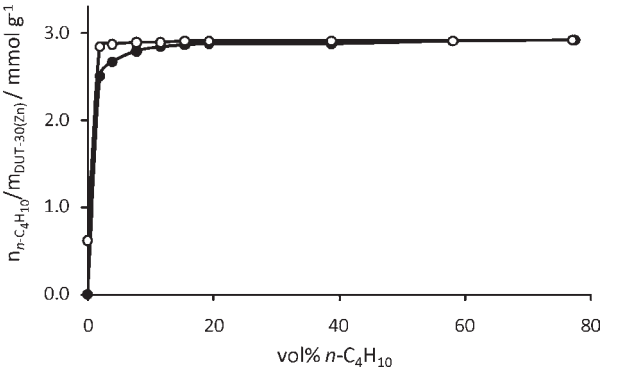

Figure 11. *n*-Butane adsorption isotherm of $Zn_2(adb)_2(dabco)$ at 20 °C.

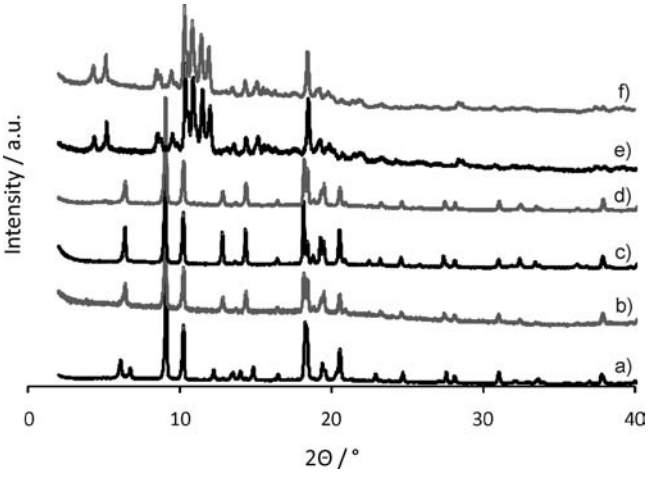

Figure 12. X-ray powder diffraction patterns: (a) compound ***K***; (b) ***K*** exposed to air for 2 weeks; (c) compound ***T***; (d) ***T*** exposed to air for 2 weeks; (e) compound ***A***; and (f) ***A*** exposed to air for 2 weeks.

Synchrotron in situ PXRD/adsorption experiments with CO_2 at various conditions are scheduled to investigate structural dynamics of the framework.

Figure 11 displays the *n*-butane adsorption isotherm of activated $Zn_2(adb)_2(dabco)$ (***A***) at 20 °C. The *n*-butane isotherm shows, as well as the nitrogen adsorption isotherm, the phenomenon of the gate-pressure. DUT-30(Zn) has a storage capacity of 3.0 mmol·g^{-1} at 77 vol % *n*-butane, which is similar to the value of $Cu_3(btc)_2$ (3.7 mmol·g^{-1})[39] again reflecting the high hydrophobicity of DUT-30(Zn).

Stability Tests. To verify the stability of $Zn_2(adb)_2(dabco)$, a de- and resolvation was accomplished several times without a great loss of crystallinity and porosity, which was controlled by powder X-ray diffraction and N_2 physisorption (Figure S5) measurements.

Also samples of compounds ***K***, ***T***, and ***A*** were exposed to laboratory ambient conditions for 2 weeks. N_2 physisorption (Figure S6) and XRD measurements (Figure 12) show that the compounds maintain their porosity and crystallinity, and are not sensitive to ambient atmosphere. However the compound ***K*** loses DMF transforming to ***T*** as described above.

The stability against water was also examined. The analysis of a water treated sample (***W***) shows that $Zn_2(adb)_2(dabco)$ can include water molecules undergoing a structural change. The water molecules incorporated in the structure cannot be completely removed by activation at 150 °C and N_2 adsorption measurement reveals the low porosity of such material (BET surface area of 40 m^2 g^{-1} ($p/p_0 = 0.1-0.3$)). Thermogravimetric analysis (Figure S8) shows that approximately 0.5 H_2O molecule per $Zn_2(adb)_2(dabco)$ was still enclosed after activation. Furthermore, the residual mass is 2.2% higher than expected, accordingly the sample already contains ZnO or $Zn(OH)_2$. Hence, a slow decomposition is proceeding during hydration.

Exchange of adsorbed water in ***W*** with DMF causes an XRD pattern identical to ***T***, but the amorphous background slightly increases (Figure S7). After exchange of water with DMF and further activation, the N_2 physisorption experiments reveal that the sample has a lower nitrogen uptake (BET surface area of 515 m^2 g^{-1}) than before (Figure S7), also evident for partial decomposition.

Thermal stability of ***K*** was investigated using thermogravimetric (TG) analysis (Figure S9). The TG plot of ***K*** illustrates that the compound starts losing solvent at temperatures slightly above ambient. At approximately 250 °C all guest molecules are removed (calcd. 23.4%). From ca. 350 °C the amine pillar ligand (dabco) disappears. At 450 °C the framework decomposes completely with elimination of the adb linker. Decarboxylation is also occurring. The calorimetric DTA curve does not exhibit any signals indicating phase transition from ***K*** to ***T***.

Conclusions. $Zn_2(adb)_2(dabco)$ is a new microporous compound which shows vast structural transformation during desolvation, resolvation, and hydration, as well as during cooling or gas physisorption. Despite 2-fold interpenetration of the network, the compound exhibits a BET surface area of 960 m^2 g^{-1} and hydrogen uptake of 1.12 wt % at −196 °C and 1 bar. Furthermore, the metal−organic framework is resistant to ambient air atmosphere, and highly hydrophobic, thus it is promising for gas storage and adsorption of volatile organics under ambient conditions.

■ ASSOCIATED CONTENT

Supporting Information. Experimental details of in situ PXRD; crystal structure of Me_2adb; synthesis description of H_2adb; additional powder patterns and isotherms; TGA and DTA curves. This material is available free of charge via the Internet at http://pubs.acs.org.

■ AUTHOR INFORMATION

Corresponding Author

*Fax: (+49)0351-46337287. E-mail: Stefan.Kaskel@chemie.tu-dresden.de.

■ ACKNOWLEDGMENT

We are grateful for the financial support of the German Research Foundation (SPP 1362), BMBF (05K10OD3), and the Helmholtz Centre Berlin (BESSY II). A special thanks goes to Dr. Gudrun Auffermann (Max Planck Institute for Chemical Physics of Solids) for performance of the elemental analyses.

■ REFERENCES

(1) Kitagawa, S.; Kitaura, R.; Noro, S. *Angew. Chem., Int. Ed.* **2004**, *43*, 2334–2375.

(2) Kaskel, S. Porous Metal-Organic Frameworks. In *Handbook of Porous Solids*, Vol. 2; Schüth, F., Sing, K. S. W., Weitkamp, J., Eds.; Wiley-VCH: Weinheim, Germany, 2002; pp 1190−1249.
(3) MacGillivray, L. R. *Metal-Organic Frameworks*; Wiley-VCH: Hoboken, NJ, 2010.
(4) Férey, G. *Stud. Surf. Sci. Catal.* **2007**, *170A*, 66–86.
(5) Klein, N.; Senkovska, I.; Gedrich, K.; Stoeck, U.; Henschel, A.; Müller, U.; Kaskel, S. *Angew. Chem., Int. Ed.* **2009**, *48*, 9954–9957.
(6) Férey, G.; Mellot-Draznieks, C.; Serre, C.; Millange, F.; Dutour, J.; Surble, S.; Margiolaki, I. *Science* **2005**, *309*, 2040–2042.
(7) Koh, K.; Wong-Foy, A. G.; Matzger, A. J. *J. Am. Chem. Soc.* **2009**, *131*, 4184–4185.
(8) Koh, K.; Wong-Foy, A. G.; Matzger, A. J. *Angew. Chem., Int. Ed.* **2008**, *47*, 677–680.
(9) Rowsell, J. L. C.; Millward, A. R.; Park, K. S.; Yaghi, O. M. *J. Am. Chem. Soc.* **2004**, *126*, 5666–5667.
(10) Collins, D. J.; Zhou, H.-C. *J. Mater. Chem.* **2007**, *17*, 3154–3160.
(11) Panella, B.; Hirscher, M.; Pütter, H.; Müller, U. *Adv. Funct. Mater.* **2006**, *16*, 520–524.
(12) Mulfort, K. L.; Farha, O. K.; Malliakas, C. D.; Kanatzidis, M. G.; Hupp, J. T. *Chem.—Eur. J.* **2010**, *16*, 276–281.
(13) (a) Küsgens, P.; Rose, M.; Senkovska, I.; Fröde, H.; Henschel, A.; Siegle, S.; Kaskel, S. *Microporous Mesoporous Mater.* **2009**, *120*, 325–330. (b) Biswas, S.; Grzywa, M.; Nayek, H. P.; Dehnen, S.; Senkovska, I.; Kaskel, S.; Volkmer, D. *Dalton Trans.* **2009**, 6487–6495.
(14) Dybtsev, D. N.; Chun, H.; Yoon, S. H.; Kim, D.; Kim, K. *J. Am. Chem. Soc.* **2004**, *126*, 32–33.
(15) Car, A.; Stropnik, C.; Peinemann, K.-V. *Desalination* **2006**, *200*, 424–426.
(16) Ma, S.; Sun, D.; Wang, X.-S.; Zhou, H.-C. *Angew. Chem., Int. Ed.* **2007**, *46*, 2458–2462.
(17) Czaja, A. U.; Trukhan, N.; Müller, U. *Chem. Soc. Rev.* **2009**, *38*, 1284–1293.
(18) Ma, L.; Abney, C.; Lin, W. *Chem. Soc. Rev.* **2009**, *38*, 1248–1256.
(19) Lee, J. Y.; Farha, O. K.; Roberts, J.; Scheidt, K. A.; Nguyen, S. B. T.; Hupp, J. T. *Chem. Soc. Rev.* **2009**, *38*, 1450–1459.
(20) Horcajada, P.; Serre, C.; Vallet-Regi, M.; Sebban, M.; Taulelle, F.; Férey, G. *Angew. Chem., Int. Ed.* **2006**, *45*, 5974–5978.
(21) An, J.; Geib, S. J.; Rosi, N. L. *J. Am. Chem. Soc.* **2009**, *131*, 8376–8377.
(22) Fletcher, A. J.; Thomas, K. M.; Rosseinsky, M. J. *J. Solid State Chem.* **2005**, *178*, 2491–2510.
(23) Dybtsev, D. N.; Chun, H.; Kim, K. *Angew. Chem., Int. Ed.* **2004**, *43*, 5033–5036.
(24) Seki, K. *Chem. Commun.* **2001**, 1496–1497.
(25) Wang, H.; Getzschmann, J.; Senkovska, I.; Kaskel, S. *Microporous Mesoporous Mater.* **2008**, *116*, 653–657.
(26) Férey, G.; Latroche, M.; Serre, C.; Millange, F.; Loiseau, T.; Percheron-Guegan, A. *Chem. Commun.* **2003**, 2976–2977.
(27) Klein, N.; Herzog, C.; Sabo, M.; Senkovska, I.; Getzschmann, J.; Paasch, S.; Lohe, M. R.; Brunner, E.; Kaskel, S. *Phys. Chem. Chem. Phys.* **2010**, *12*, 11778–11784.
(28) Li, D.; Kaneko, K. *Chem. Phys. Lett.* **2001**, *335*, 50–56.
(29) Chun, H.; Dybtsev, D. N.; Kim, H.; Kim, K. *Chem.—Eur. J.* **2005**, *11*, 3521–3529.
(30) Eddaoudi, M.; Kim, J.; Rosi, N.; Vodak, D.; Wachter, J.; O'Keeffe, M.; Yaghi, O. M. *Science* **2002**, *295*, 469–472.
(31) Ma, S.; Sun, D.; Forster, P. M.; Yuan, D.; Zhuang, W.; Chen, Y.-S.; Parise, J. B.; Zhou, H.-C. *Inorg. Chem.* **2009**, *48*, 4616–4618.
(32) Palatinus, L.; Chapuis, G. *J. Appl. Crystallogr.* **2007**, *40*, 786–790.
(33) Sheldrick, G. M. *Acta Crystallogr.* **2008**, *A64*, 112–122.
(34) (a) Van der Sluis, P.; Spek, A. L. *Acta Crystallogr., Sect. A* **1990**, *A46*, 194–201.(b) Spek, A. L. *PLATON, A Multipurpose Crystallographic Tool*; Utrecht University: Utrecht, The Netherlands, 2008.
(35) (a) Chen, B.; Ma, S.; Hurtado, E. J.; Lobkovsky, E. B.; Zhou, H.-C. *Inorg. Chem.* **2007**, *46*, 8490. (b) Xue, M.; Ma, S.; Jin, Z.; Schaffino, R. M.; Zhu, G.-S.; Lobkovsky, E. B.; Qiu, S.-L.; Chen, B. *Inorg. Chem.* **2008**, *47*, 6825.
(36) Farha, O. K.; Malliakas, C. D.; Kanatzidis, M. G.; Hupp, J. T. *J. Am. Chem. Soc.* 2010, *132*, 950–952.
(37) Bureekaew, S.; Sato, H.; Matsuda, R.; Kubota, Y.; Hirose, R.; Kim, J.; Kato, K.; Takata, M.; Kitagawa, S. *Angew. Chem., Int. Ed.* **2010**, *49*, 7660–7664.
(38) Park, K. S.; Ni, Z.; Coté, A. P.; Choi, J. Y.; Huang, R.; Uribe-Romo, F. J.; Chae, H. K.; ÓKeeffe, M.; Yaghi, O. M. *Proc. Natl. Acad. Sci. U. S. A.* **2006**, *103*, 10186–10191.
(39) Klein, N.; Henschel, A.; Kaskel, S. *Microporous Mesoporous Mater.* **2010**, *129*, 238–242.